



Universidad Autónoma
de Madrid

Biblos-e Archivo
Repositorio Institucional UAM

Repositorio Institucional de la Universidad Autónoma de Madrid

<https://repositorio.uam.es>

Esta es la **versión de autor** del artículo publicado en:
This is an **author produced version** of a paper published in:

ACS Nano 12.5 (2018): 4362-4368

DOI: <https://doi.org/10.1021/acsnano.7b09189>

Copyright: © 2018 American Chemical Society.

El acceso a la versión del editor puede requerir la suscripción del recurso

Access to the published version may require subscription

Lifetime-Encoded Infrared-Emitting Nanoparticles for *In Vivo* Multiplexed Imaging

Dirk H. Ortgies^{†‡}, Meiling Tan[‡], Erving C. Ximendes[†], Blanca del Rosal[‡], Jie Hu[†], Lei Xu[‡], Xindong Wang[‡], Emma Martín Rodríguez^{†‡}, Carlos Jacinto[†], Nuria Fernandez^{‡‡}, Guanying Chen^{†*} and Daniel Jaque^{†‡*}

[†] Fluorescence Imaging Group, Universidad Autonoma de Madrid, Madrid 28049, Spain

[‡] MIIT Key Laboratory of Critical Materials Technology for New Energy Conversion and Storage, School of Chemistry and Chemical Engineering & Key Laboratory of Micro-systems and Micro-structures, Ministry of Education, Harbin Institute of Technology, 150001 Harbin, People's Republic of China.

[‡] Grupo de Fotônica e Fluidos Complexos, Instituto de Física, Universidade Federal de Alagoas, 57072-900 Maceió-AL, Brazil

^{‡‡} Fluorescence Imaging Group, Departamento de Fisiología, Facultad de Medicina, Avda. Arzobispo Morcillo 2, Universidad Autónoma de Madrid, 28029 Madrid, Spain.

[‡] Centre for Micro-Photonics, Faculty of Science, Engineering and Technology, Swinburne University of Technology, PO Box 218, Hawthorn, VIC 3122, Australia

[‡] Nanobiology Group, Instituto Ramón y Cajal de Investigación Sanitaria, IRYCIS, Ctra. Colmenar km. 9.100, Madrid 28034, Spain.

KEYWORDS: *infrared bioimaging, in vivo multiplexing, rare-earth-doped nanoparticles, lifetime spectroscopy, biological windows.*

ABSTRACT: Advanced diagnostic procedures are required to satisfy the continuously increasing demands of modern biomedicine while also addressing the need for cost reduction in public health systems. The development of infrared luminescence-based techniques for *in vivo* imaging is emerging as a reliable alternative to traditional imaging techniques, applicable with simpler and more cost-effective apparatus. In order to further improve the information provided by *in vivo* luminescence images, the design and fabrication of enhanced infrared-luminescent contrast agents is required. In this work, we demonstrate how simple dopant engineering can lead to infrared-emitting rare-earth-doped nanoparticles with tunable (0.1-1.5 ms) and medium-independent luminescence lifetimes. The combination of these tunable nanostructures with time-gated infrared imaging and time domain analysis is employed to obtain multiplexed *in vivo* images that are used for complex biodistribution studies.

Fluorescence has received renewed interest for *in vivo* imaging in the past few years thanks to the development of biocompatible fluorescent contrast agents operating in the infrared.¹⁻³ In particular, the spectral ranges known as biological windows (650-950 nm, the first biological window, NIR I; 1000-1350 nm, the second biological window, NIR II) have been intensively explored due to the fact that biological tissues are partially transparent to radiation wavelengths incident on them.^{4,5} Additionally, the decrease in both light scattering and tissue autofluorescence at longer wavelengths⁶⁻⁸ enables the minimally invasive visualization of embedded organs and vascular structures with a very high spatial resolution.⁹ Indeed, NIR-II imaging has been successfully employed in small animal models for intravital imaging, dynamic

biodistribution studies, tumor diagnosis and transcranial visualization of cerebral vasculature.¹⁰⁻¹⁵ However, the limited number of fluorescent probes operating in the biological windows has prevented the development of *in vivo* NIR multiplexed imaging, which requires an accurate isolation of the signals generated by different fluorophores in a single image.^{16,17} *In vivo* fluorescence multiplexing would, in principle, enable simultaneously studying the targeting efficiency of different drugs or nanoparticles (hereafter, NPs) with different surface functionalizations, multiple tumor targeting, and also increasing the overall throughput of imaging-based diagnostic techniques. However, due to a significant degree of overlap between the emission spectra of different infrared optical probes currently available (such as carbon nanostructures, organic

dyes, semiconductor NPs -quantum dots- and lanthanide-doped NPs), their application in spectral multiplexing has remained unaccomplished, as the emission signal generated by each one of the fluorophores could not be easily isolated.

Fluorescence multiplexing does not have to be necessarily performed in the spectral domain. Other spectroscopic properties can also be used to elucidate between several fluorophores.¹⁸⁻²¹ Research performed with visible-emitting contrast agents indicates the suitability of lifetime multiplexing for straightforward discrimination between fluorophores, providing the possibility of an increased throughput of *in vitro* multicolor assays.²²⁻²⁸ Extending the applicability of this approach to *in vivo* imaging requires the development of NIR-operating biocompatible contrast agents with significantly different fluorescence lifetimes. The use of NIR-emitting NPs for lifetime-based multiplexed imaging of living cells was already successfully demonstrated but *in vivo* high penetration lifetime-based multiplexed imaging is still something unachieved.²⁹ Lanthanide-doped NPs constitute ideal candidates for this purpose, as their spectral and morphological properties can be precisely controlled by adjusting their synthesis procedure. Their characteristically long fluorescence lifetimes (in the micro-to-millisecond range), which makes them particularly useful for autofluorescence-free bioimaging through time-gated detection,³⁰⁻³² can also be tuned.³³ As demonstrated with visible-emitting upconverting NPs, different concentrations of dopant ions can generate nanoparticles with different lifetimes but identical crystal structure and morphology.²⁴ This is particularly important when aiming to apply them as *in vivo* contrast agents, as size is a key factor in NP biodistribution.^{34,35} Despite these promising facts, the possibility of lifetime tunability in NIR-operating lanthanide-doped NPs and their applicability for *in vivo* multiplexed imaging in the time domain remains unexplored.

In this work we demonstrate the feasibility of *in vivo* NIR multiplexed imaging in the time domain by using small-sized NaYF₄:Yb,Nd@CaF₂ core/shell NPs as contrast agents. The CaF₂ was used as the shell material not only because it has a low lattice mismatch with the core, broad spectral range of optical transparency, and high stability in aqueous environments, but also because its constituents (calcium and fluoride ions) are common components of bone and teeth, which can enhance the biocompatibility of the resulting core/shell NPs.³⁶ Lifetime tuning is achieved through an adequate dopant engineering that allows modulation of energy transfer, radiative and nonradiative probabilities. High contrast multiplexed *in vivo* imaging in the NIR-II is achieved by the straightforward combination of lifetime tunable NaYF₄:Yb,Nd@CaF₂ core/shell NPs with a simple time-gated *in vivo* imaging setup and a custom-made software for image analysis.

RESULTS/DISCUSSION

Six different samples of NaY_{0.9-x}Yb_{0.1}Nd_xF₄@CaF₂ core/shell NPs with Nd³⁺ concentrations $x = 0.1, 0.2, 0.3, 0.5, 0.8$ and 0.9 were synthesized by a thermal decomposition method and then functionalized with a poly(acrylic acid) coating (see the Methods Section).

Figures 1(a) and 1(b) show the representative TEM and high-angle annular dark-field (HAADF) scanning transmission electron microscopy (STEM) images corresponding to the core/shell NPs with a Nd³⁺-doping level of $x = 0.1$. In **Figure 1(b)** the presence of the spherical core and cubic shell is indicated. **Figure 1(c)** shows the room temperature emission spectra generated by the NaYF₄:Yb,Nd@CaF₂ core/shell NPs with different Nd³⁺-dopant levels under continuous wave 808 nm excitation, so that only Nd³⁺ ions are optically excited. All spectra show two emission bands centered at around 980 and 1350 nm. The band centered at 980 nm can be ascribed to the ²F_{5/2}→²F_{7/2} and the ⁴F_{3/2}→⁴I_{11/2} transitions of Yb³⁺ and Nd³⁺, respectively. On the other hand, the one centered at around 1350 nm corresponds to the ⁴F_{3/2}→⁴I_{13/2} transition of Nd³⁺. The presence of emission bands generated by Yb³⁺-ions evidences an efficient Nd³⁺→Yb³⁺ energy transfer. Both the overall emitted intensity and the ratio between emitted intensities at around 980 and 1350 nm (hereafter denoted by $R_{Yb/Nd}$) are strongly dependent on the Nd³⁺ content (see Supporting Information). A maximum overall emitted intensity was achieved for a Nd³⁺ content of $x = 0.2-0.3$. This can be explained considering that low concentrations would lead to weak absorption of 808 nm radiation, whereas larger concentrations will activate energy diffusion and cross relaxation process, thus preventing an efficient Nd³⁺→Yb³⁺ energy transfer. Meanwhile, $R_{Yb/Nd}$ increases for Nd³⁺ concentrations below $x = 0.2$, due to an enhancement of the Nd³⁺→Yb³⁺ energy transfer efficiency. Higher Nd³⁺ concentrations lead to a decrease in $R_{Yb/Nd}$, indicating a reduction in the contribution of Yb³⁺ emission to the overall intensity, which is likely a consequence of the activation of the Nd³⁺←Yb³⁺ energy back-transfer processes, as schematically illustrated in Section S4 of the Supporting Information. Hence, it is demonstrated that spectral properties can be tailored through adequate doping. It is important to point out that all the synthesized NPs were highly homogeneous and showed no signs of agglomeration (see Supporting Information for a detailed characterization). Analysis of TEM images reveals very similar size histograms for all the samples, as summarized in **Figure 1(d)**, where the average particle diameter as a function of the Nd³⁺ content is shown. Furthermore, as discussed in **Section S2** of the Supporting Information, the core size remains almost identical (around 6-7 nm) for all dopant levels. Thus, different doping modifies spectral properties without affecting the morphological properties of NaYF₄:Yb,Nd@CaF₂ core/shell NPs.

The fluorescence decay curves of the samples used in this work, obtained at 980 nm under 808 nm excitation, are presented in **Figure 2(a)**. The results indicate a strong dependence between the decay time and the Nd³⁺ content. The concentration dependence of the fluorescence decay time (calculated as $\tau = \int I_{em}(t)dt/I_0$, where $I_{em}(t)$ is the emitted intensity after a time t in respect to excitation pulse and I_0 is the emitted intensity at $t = 0$) is shown in **Figure 2(b)**. Higher contents in Nd³⁺ result in shorter fluorescence decay times, although the trend is not linear. Data included in **Figure 2(b)** shows the possibility of tuning the fluorescence lifetime in the range of 1.4-0.2 ms through dopant engineering. This concentration-induced reduction

in the fluorescence lifetime can be explained by the activation of $\text{Nd}^{3+} \leftarrow \text{Yb}^{3+}$ energy back-transfer processes, which act as a non-radiative de-excitation channel for Yb^{3+} ions. The Nd^{3+} luminescence decay time also decreases markedly with increasing Nd^{3+} content, as shown in Section S4 in the Supporting Information. This is due to the activation of energy migration and cross relaxation processes between adjacent Nd^{3+} ions.

The influence of the medium on the luminescence lifetime of $\text{NaYF}_4:\text{Yb,Nd}@\text{CaF}_2$ core/shell NPs was evaluated, as it would limit their applicability for *in vivo* imaging in the time domain. **Figure 2(c)** shows the fluorescence decay curves of $\text{NaYF}_4:\text{Yb,Nd}@\text{CaF}_2$ with a Nd^{3+} content $x = 0.5$ as obtained in different aqueous environments (deionized water, phosphate-buffered-saline (PBS), acidic and basic dispersions). Details about these measurements can be found in the Methods section. The resulting fluorescence lifetimes obtained in these media are almost identical (**Figure 2(d)**). This indicates that the fluorescence lifetime of our $\text{NaYF}_4:\text{Yb,Nd}@\text{CaF}_2$ core/shell NPs is virtually independent of the environment. This outstanding feature is a direct consequence of their core/shell structure, as the CaF_2 shell avoids direct interaction between the emitting ions (located at the NaYF_4 core) and the ions surrounding the NPs, especially the OH^- ion under basic conditions that is regularly involved in the quenching of rare-earth-doped NaYF_4 NPs.

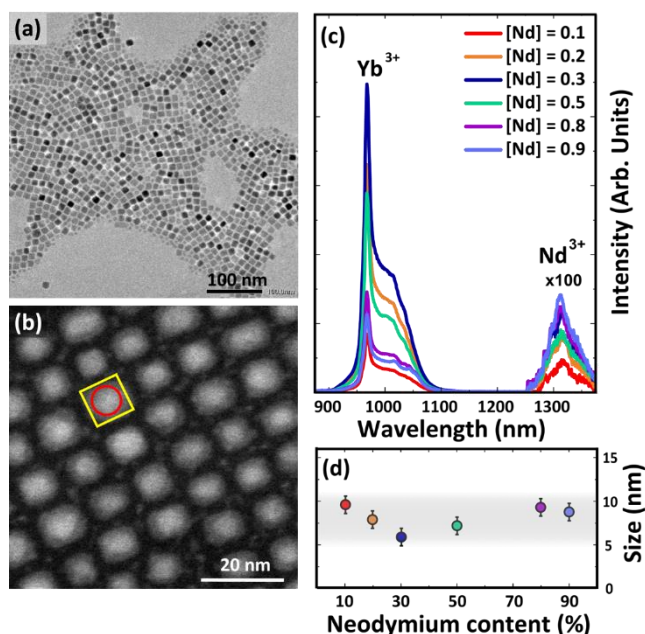


Figure 1. Morphological and spectroscopic characterization: (a) TEM and (b) HAADF STEM images corresponding to the $\text{NaY}_{0.9-x}\text{Yb}_{0.1}\text{Nd}_x\text{F}_4@\text{CaF}_2$ core/shell NPs with $x = 0.1$. In (b) the red circle and yellow square indicate the spherical core and the cubic shell, respectively. (c) Room temperature emission spectra corresponding to the $\text{NaYF}_4:\text{Yb,Nd}@\text{CaF}_2$ NPs with different Nd^{3+} dopant concentrations. (d) Average particle size as a function of the Nd^{3+} doping level (calculated from TEM images included in Supporting Information).

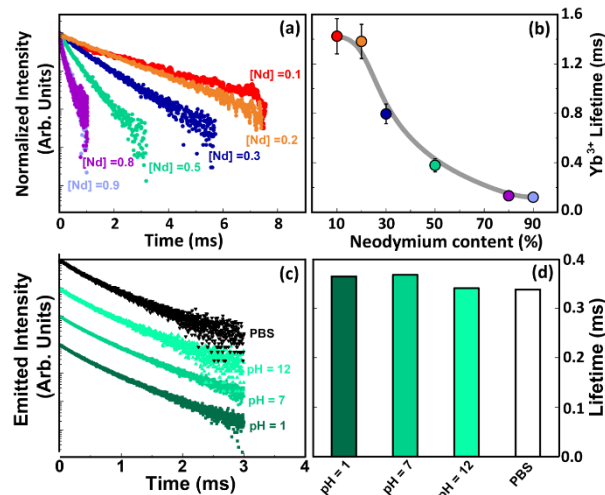


Figure 2. Fluorescence lifetimes: (a) Fluorescence decay curves obtained for the $\text{NaYF}_4:\text{Yb,Nd}@\text{CaF}_2$ core/shell NPs with six different Nd^{3+} dopant levels. Excitation was performed at 808 nm and the observed emission wavelength was 980 nm. (b) Concentration dependence of the fluorescence lifetime of the $\text{NaYF}_4:\text{Yb,Nd}@\text{CaF}_2$ NPs. The dots are experimental data obtained from (a) and the line is a guide for the eyes. (c). Fluorescence decay curves obtained for $\text{NaYF}_4:\text{Yb,Nd}@\text{CaF}_2$ NPs with a neodymium content of $x = 0.5$ obtained in different aqueous media. Excitation and emission wavelengths were set to 808 and 980 nm, respectively. The decay curves were translated vertically for better visualization. (d) Fluorescence lifetime values of the same NPs with a neodymium content of $x = 0.5$ obtained from the experimental data included in (c).

Multiplexed *in vivo* images in the second biological window.

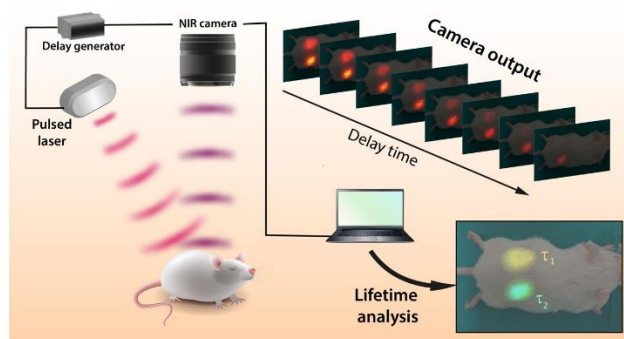


Figure 3. Schematic diagram of the experimental set up used for the acquisition of *in vivo* lifetime images: Image acquisition is synchronized with the excitation pulse. Analysis of fluorescence images acquired with different time delays in respect to laser pulse leads to lifetime images that allows for *in vivo* multiplexing in the time domain. The fluorescence images obtained for different time delays as well as the lifetime image included as an example correspond to real measurements performed on a mouse with two subcutaneous injections of $\text{NaYF}_4:\text{Yb,Nd}@\text{CaF}_2$ NPs with neodymium contents of $x = 0.3$ and $x = 0.5$ with fluorescence lifetimes of $\tau_1 = 0.7$ ms and $\tau_2 = 0.4$ ms, respectively.

The ability of our $\text{NaYF}_4:\text{Yb,Nd}@\text{CaF}_2$ core/shell NPs with tunable fluorescence lifetime for *in vivo* multiplexed imaging in the second biological window was evaluated in

CD1 mice using the experimental setup shown in **Figure 3**. A time-modulated 808 nm diode laser was used to illuminate the animal under study, which was imaged by a Peltier-cooled InGaAs camera so as to detect the NP

emission. Between the laser driver and the camera acquisition, an electronic delay circuit allows to adapt the elapsed time between the end of each laser pulse and the image acquisition in the 10 μ s-3 ms range. Further details

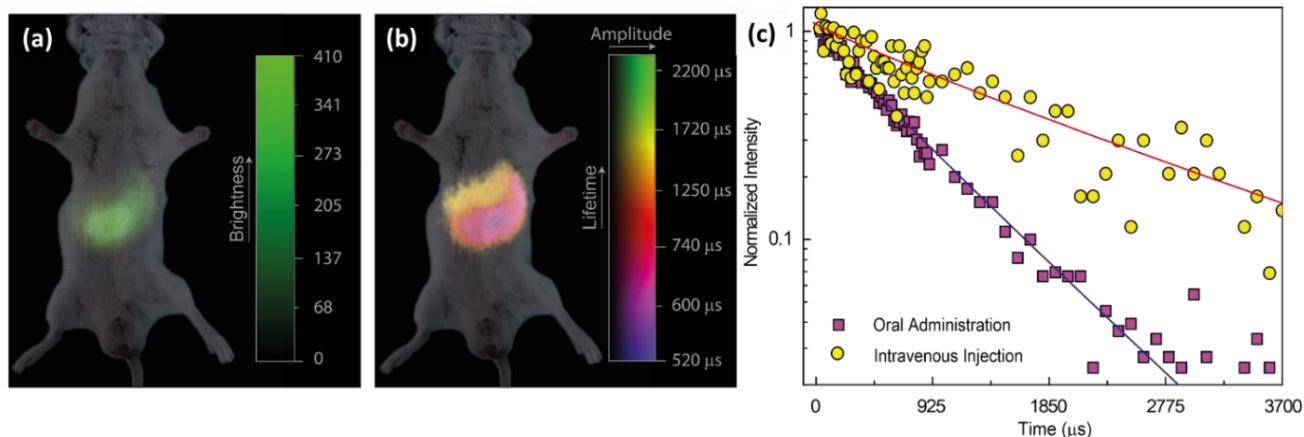


Figure 4. *In vivo* multiplexed lifetime imaging: (a) Intensity-based infrared image of a mouse after oral and intravenous injection of $\text{NaY}_{0.9-x}\text{Yb}_{0.1}\text{Nd}_x\text{F}_4@\text{CaF}_2$ NPs with a Nd^{3+} content of $x = 0.3$ and 0.2 , respectively. (b) Lifetime-based image of same mouse as in (a). The different location of the two types of NPs is evidenced. (c) Fluorescence decay curves obtained at two different locations corresponding to $\text{NaYF}_4:\text{Yb,Nd}@\text{CaF}_2$ core/shell NPs administrated orally and intravenously. Symbols are experimental data and solid lines are best exponential fits.

about the experimental set-up can be found in the Methods section and the literature.³⁰ The time resolution of our time gating system is discussed in the Supporting Information where it is concluded that this is close to ± 15 μ s. The fluorescence images obtained for different time delays are then analyzed in the time domain by a custom-made software that provides a lifetime image, as schematically shown in **Figure 3**. More details about the software used for image analysis can be found in the Supporting Information in which we also provide the lifetime images obtained for the different $\text{NaYF}_4:\text{Yb,Nd}@\text{CaF}_2$ core/shell NPs used in this work. Multiplexed infrared imaging is here demonstrated by performing a double administration of $\text{NaYF}_4:\text{Yb,Nd}@\text{CaF}_2$ core/shell NPs. The mouse under study received 200 μ L of an aqueous dispersion of NPs with a Nd^{3+} content of $x = 0.3$ ($\tau = 0.7$ ms) through oral administration and an intravenous injection of 100 μ L of a PBS dispersion of NPs with a Nd^{3+} content $x = 0.2$ ($\tau = 1.3$ ms). Details about the administration procedure can be found in the Methods section. At this point we would like to remark that for *in vivo* experiments we choose $x = 0.2$ and 0.3 because, according to **Figure 2(b)**, these samples lead to the largest pronounced lifetime change with the minimum concentration variation. This, in turn, ensures good contrast in the time domain while keeping the luminescence intensity at similar level. **Figure 4(a)** shows the intensity-based fluorescence image of the mouse after being inoculated with the two types of NPs. In this image, obtained with no delay between laser excitation and acquisition, only fluorescence generated from the top part of the abdomen can be observed. This clearly suggests accumulation of the administrated NPs in the organs located in this area, including stomach, liver and spleen. Although the NP localization can be traced from the image **Figure 4(a)**, no further information can be obtained from it. Particularly,

the possible different biodistribution routes followed by NPs after oral or intravenous administration cannot be elucidated. The fluorescence lifetime image is shown in **Figure 4(b)**. In this case, the different biodistribution of $\text{NaYF}_4:\text{Yb,Nd}@\text{CaF}_2$ core/shell NPs after oral and intravenous administration is evidenced. The NPs presenting the longer lifetime (intravenously administrated) are accumulated in a large and circular area at the upper part of the abdomen. Comparing this with the NIR-II *in vivo* images obtained in previous works we can associate this localization to NPs accumulation at the liver, which is consistent with the results reported in the literature for intravenously injected lanthanide-doped NPs,³⁷ as well as with the *ex vivo* images included in the Supporting Information. **Figure 4(b)** also reveals that the shorter lifetime NPs followed a completely different biodistribution pattern. They also accumulate in the upper part of the abdomen but in a smaller area, whose location and shape suggests NP accumulation in the stomach. This result is consistent with the fact that these NPs were orally administrated. The accumulation at different organs of orally and intravenously injected NPs is further evidenced by the decay curves extracted from fluorescence images as obtained at two different spots (corresponding to the stomach and liver) shown in **Figure 4(c)**. The same technique can also be applied to distinguish between more than two different types of $\text{NaYF}_4:\text{Yb,Nd}@\text{CaF}_2$ core/shell NPs. Indeed, we were able to distinguish three different nanoparticles by *in vivo* multiplexing imaging as it is shown in **Section S6** of Supporting Information. In addition, the $\text{NaYF}_4:\text{Yb,Nd}@\text{CaF}_2$ core/shell NPs here used showed no toxicity effects at the *in vivo* level as is evidenced by the results included in **Section S8** of Supporting Information.

CONCLUSIONS

In summary, this work demonstrates how acquisition of *in vivo* multiplexed images in the second biological window is possible by combining time-gated imaging techniques and lanthanide-doped NPs with tunable fluorescence lifetime. Dopant engineering enables continuous tuning of the infrared fluorescence lifetime of NaYF₄:Yb,Nd@CaF₂ NPs from 1.4 ms down to 100 μ s while preserving their size and shape. In addition, the core/shell structure prevents the interaction between luminescent ions and their environment, making the fluorescence lifetime a robust and invariant parameter for *in vivo* imaging experiments. The demonstration of *in vivo* animal multiplexed lifetime imaging herein provided, enables an accurate and unequivocal distinction between NPs and allows the determination of the different biodistribution pathways followed by NPs inoculated *via* different routes. The presented results constitute a step towards the design of diagnostic tools based on the acquisition of multiplexed *in vivo* images in the biological windows.

METHODS/EXPERIMENTAL

Synthesis of α -NaYF₄: 10% Yb³⁺, x% Nd³⁺ (x=10, 20, 30, 50, 90) core nanoparticles: The α -NaYF₄: Yb³⁺, Nd³⁺ core nanoparticles (NPs) were prepared *via* the decomposition of rare earth trifluoroacetates at a high temperature. In a typical procedure, 0.05 mmol Yb₂O₃, x mmol Nd₂O₃ (x = 0.05, 0.1, 0.15, 0.4) and (0.45-x) mmol Y₂O₃ were loaded into a 250 mL flask that contained 5 mL deionized water and 5 mL TFA, and heated to 90 °C for 1 hour to yield a clear solution. Then, the resulting clear solution was evaporated under argon purge to get muddy powdered RE(TFA)₃. Subsequently, 8 mL OA, 8 mL OM, 12 mL ODE and 2 mmol NaTFA were added into the flask. The solution was heated to 120 °C and kept at that temperature for 30 min to remove water and oxygen, followed by heating up to 300 °C for 30 min and letting cool down to room temperature under an inert argon atmosphere. The resulting nanoparticles were precipitated by adding 20 mL ethanol to the cooled reaction flask. After centrifugal washing with ethanol for three times, the collected white powder was finally dispersed in 10 mL hexane for further uses.

Synthesis of α -NaYF₄: 10% Yb³⁺, x% Nd³⁺ (x=10, 20, 30, 50, 80)@CaF₂ core-shell nanoparticles: The core-shell nanoparticles were prepared *via* a seed-mediated epitaxial growth process, involving the use of α -NaYF₄: 10% Yb³⁺, x% Nd³⁺ core as the seed and the growth in the shell precursor solution. To prepare the shell precursor, firstly, 2 mmol CaO with 5 mL deionized water and 5 mL TFA were added to a 250 mL flask and heated at 90 °C for 1 hour to produce a clear solution. This solution was then evaporated to yield the shell precursor of calcium trifluoroacetate (Ca(TFA)₂). Next, 0.5 mmol NaYF₄: 10% Yb³⁺, x% Nd³⁺ (x=10, 20, 30, 50, 80) core nanoparticles, 7 mL OA and 7 mL ODE were all added to the flask. The solution was then heated to 120 °C for 30 min to remove water and oxygen, followed by heating up to 300 °C for 60 min before naturally cooling down. The whole process was carried out under argon environment and with a magnetic stirring rate of 250 rpm. The resulting core-shell nanoparticles were precipitated by adding 20 mL ethanol to the cooled reaction flask. After centrifugal washing with ethanol for three times, the collected core-shell NPs was finally dispersed in 10 mL hexane for further uses.

Synthesis of poly(acrylic acid) coated NPs: Firstly, 5 mL NPs dispersed in hexane were mixed with a 5 mL *N,N*-Dimethylformamide (DMF) solution of nitrosonium tetrafluoroborate (NOBF₄) (0.1 M) at room temperature. The mixture was then gently shaken until NP precipitation was observed. Subsequently, toluene and hexane (1:1, volume) were added into the solution, which was centrifuged at 10000 rpm for 10 min. The precipitate was collected and dispersed in 5 mL DMF. In the second step, 250 mg poly(acrylic acid) (MW=18, 000) was added to the 5 mL DMF solution of NOBF₄-treated NPs, which was then heated to 80 °C and kept at this temperature for 30 min under vigorous stirring. After that, the NPs were precipitated by adding acetone, washed with ethanol, and finally dispersed in distilled water for further uses.

Lifetime measurements: Room temperature lifetime measurements were performed by using an Optical Parametric Oscillator (Quanta Ray) pumped by a frequency tripled Nd:YAG laser operating at 355 nm. The Optical Parametric Oscillator operates at 800 nm wavelength and provides 10 ns pulses with an average energy of 0.2 J and with a repetition rate of 10 Hz. The luminescence was collected and spectrally filtered by a high brightness monochromator (Shamrock 163 from Andor). Time evolution was recorded by an infrared photomultiplier (Hamamatsu H1033C) connected to a digital oscilloscope (Le Croy Wave Runner 500).

For the lifetime measurements at different pHs first the standard aqueous dispersion (20 mg/mL) at pH 7 was measured and then brought to pH 1 through the addition of 1-2 drops of concentrated HCl and the sample was measured again. The NPs were recovered by centrifugation (15 min, 6000 rpm) and redispersed in PBS (20 mg/mL) after washing with H₂O. This dispersion was employed for the next lifetime measurement and then the pH was increased to 12 with 1-2 mg of solid NaOH for the final measurement.

Fluorescence Imaging: All fluorescence images were collected using an InGaAs CCD camera with enhanced sensitivity in the 1000–1700 nm spectral range (Xeva1.7-320). Optical excitation was achieved using a fiber-coupled 808 nm laser diode (LIMO) with a maximum output power of 10 W. The laser diode was electronically modulated providing 10 ms pulses with a pulse-to-pulse separation of 35 ms. The tunable time delay between the end of laser pulse and camera acquisition was introduced by using a custom-made electronic delay circuit. A long pass filter with cutoff wavelength at 850 nm (Thorlabs FEL850) was employed to remove the 808 nm pump background. The laser power was 10 W and the spot size was close to 50 cm². This leads to a peak power density of 0.2 W/cm². Pulse width is 10 ms leading to a pulse energy of 0.1 J. Pulse separation is 35 ms so that pulse repetition rate is 28 Hz. This leads to an average power of 0.035 W and, therefore, to an average power density of 0.7 mW/cm². Both the instantaneous and average power densities are well below the damage threshold that is typically assumed, for 800 nm radiation, to be 1 W/cm².

Time domain analysis of fluorescence images: For the sake of brevity, the principles behind the custom-made software that was used to analyze the fluorescence images in the time domain are described in the Supporting Information.

Animal experiments: The *in vivo* experiments carried out in this work were approved by the Ethics Committee from Universidad Autónoma de Madrid (CEI) and complied with the

principles of good laboratory animal care following the European Directive for the protection of animals used for scientific purposes. A CD1 female mouse (weight, 35 g; age, 12 weeks) was used. Administration of NPs directly into the stomach was achieved by oral gavage using a stainless steel bulb tipped gavage needle attached to a syringe in the awake mouse gently restrained. Intravenous injection was performed using the technique of retro-orbital injection with a 26-G insulin needle and syringe to deliver the NPs in the anesthetized mouse. For the subcutaneous injection, 200 μ L of an aqueous dispersion (20 mg mL⁻¹) of NPs was used. A 25 gauge sterile needle was inserted to a depth of 1 cm under the pocket made by gently pulling up the skin over the flank. The injection depth was estimated to be 1 mm. Isoflurane was used as inhalant anesthetic (4% induction, 1% maintenance) and the *in vivo* images were obtained in the anesthetized animal. After the experiments, euthanasia was performed under isoflurane.

ASSOCIATED CONTENT

Supporting Information. Further Information about the lifetime analysis in the time domain, morphological and compositional characterization of the NPs, additional multiplexed *in vivo* and *ex vivo* images as well as *in vivo* toxicity data can be found in the Supporting Information. This material is available free of charge *via* the Internet at <http://pubs.acs.org>.

AUTHOR INFORMATION

Corresponding Authors

E-mails: chengguanying@hit.edu.cn, daniel.jaque@uam.es

Author Contributions

Dirk Ortgies, Emma Martín Rodríguez and Nuria Fernandez performed the animal experiments and contributed to the data analysis and to manuscript preparation. Meiling Tan, Lei Xu, Xindong Wang, and Guanying Chen conceived the idea, synthesized and characterized the luminescent nanoparticles. Jie Hu performed the spectroscopic characterization. Erving C. Ximendes and Carlos Jacinto developed the home-made software for the time domain analysis of fluorescence images. Blanca del Rosal and Daniel Jaque analyzed the results and wrote the manuscript. Guanying Chen and Daniel Jaque directed the project.

Funding Sources

Spanish Ministry of Economy and Competitiveness, Spanish National Health Insitutie (Instituto de Salud Carlos III), Brazilian agencies CAPES (Coordenação de Aperfeiçoamento de Pessoal de Nível Superior) and CNPq (Conselho Nacional de Desenvolvimento Científico de Tecnológico). National Natural Science Foundation of China, Fundamental Research Funds for the Central Universities, China.

ACKNOWLEDGMENT

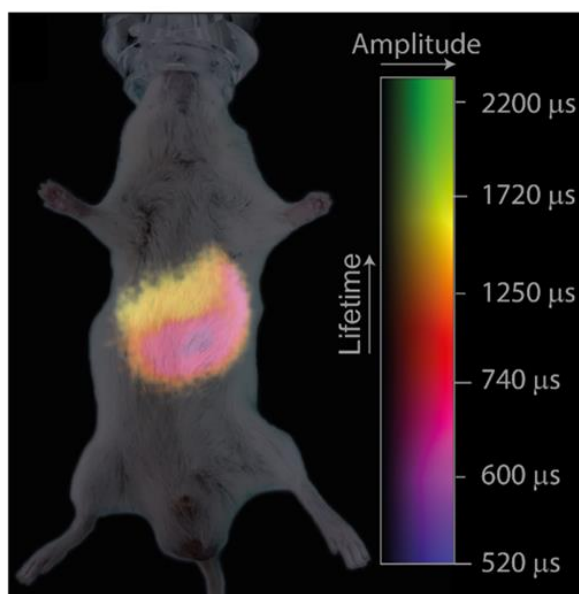
This work has been partially supported by the Ministerio de Economía y Competitividad de España (MAT2016-75362-C3-1-R), by the Instituto de Salud Carlos III (PI16/00812), by Comunidad Autónoma de Madrid (B2017/BMD-3867RENIM-CM), by the European Comission (NanoTBTech), cofinanciado con Fondos Estructurales de la Union Europea, and also by COST action CM1403. This work is also supported by the grants from the National Natural Science Foundation of China (51672061) and the Fundamental Research Funds for the

Central Universities, China (HIT.BRETIV.201503). Jie Hu acknowledges the scholarship from the China Scholarship Council (No. 201506650003). Dirk H. Ortgies is grateful to the Spanish Ministry of Economy and Competitiveness for a Juan de la Cierva scholarship (No. FJCI-2014-21101) and the ISCIII for a Sara Borrell scholarship (No. CD17/00210). E.C.X. was supported by a PhD scholarship from CNPq and by the PVE A077/2013 project by means of a joined PhD program developed at the Universidad Autónoma de Madrid, Spain. D.J. is the PVE (Pesquisador Visitante Especial) of the Project A077/2013.

REFERENCES

- Hong, G.; Antaris, A. L.; Dai, H., Near-Infrared Fluorophores for Biomedical Imaging. *Nat. Biomed. Eng.* **2017**, 1, 0010.
- Jaque, D.; Richard, C.; Viana, B.; Soga, K.; Liu, X.; García Solé, J., Inorganic Nanoparticles for Optical Bioimaging. *Adv. Opt. Photonics* **2016**, 8, 1-103.
- Lin, Q. Q.; Wang, Z. P.; Young, M.; Patel, J. B.; Milot, R. L.; Maestro, L. M.; Lunt, R. R.; Snaith, H. J.; Johnston, M. B.; Herz, L. M., Near-Infrared and Short-Wavelength Infrared Photodiodes Based on Dye-Perovskite Composites. *Adv. Funct. Mater.* **2017**, 27, 1702485.
- Bashkatov, A.; Genina, E.; Kochubey, V.; Tuchin, V., Optical Properties of Human Skin, Subcutaneous and Mucous Tissues in the Wavelength Range from 400 to 2000 nm. *J. Phys. D: Appl. Phys.* **2005**, 38, 2543-2555.
- Smith, A. M.; Mancini, M. C.; Nie, S., Second Window for *in Vivo* Imaging. *Nat. Nanotechnol.* **2009**, 4, 710-711.
- Jacques, S. L., Optical Properties of Biological Tissues: A Review. *Phys. Med. Biol.* **2013**, 58, R37-R61.
- Frangioni, J. V., *In Vivo* Near-Infrared Fluorescence Imaging. *Curr. Opin. Chem. Biol.* **2003**, 7, 626-634.
- del Rosal, B.; Villa, I.; Jaque, D.; Sanz-Rodríguez, F., *In Vivo* Autofluorescence in the Biological Windows: The Role of Pigmentation. *Journal of Biophotonics* **2016**, 9, 1059-1067.
- Hemmer, E.; Benayas, A.; Legare, F.; Vetrone, F., Exploiting the Biological Windows: Current Perspectives on Fluorescent Bioprobes Emitting above 1000 nm. *Nanoscale Horizons* **2016**, 1, 168-184.
- Benayas, A.; del Rosal, B.; Pérez-Delgado, A.; Santacruz-Gómez, K.; Jaque, D.; Hirata, G. A.; Vetrone, F., Nd:YAG Near-Infrared Luminescent Nanothermometers. *Adv. Opt. Mater.* **2015**, 3, 687-694.
- Hong, G.; Lee, J. C.; Robinson, J. T.; Raaz, U.; Xie, L.; Huang, N. F.; Cooke, J. P.; Dai, H., Multifunctional *In Vivo* Vascular Imaging Using Near-Infrared II Fluorescence. *Nat. Med.* **2012**, 18, 1841-1846.
- Hong, G. S.; Diao, S.; Chang, J. L.; Antaris, A. L.; Chen, C. X.; Zhang, B.; Zhao, S.; Atochin, D. N.; Huang, P. L.; Andreasson, K. I.; Kuo, C. J.; Dai, H. J., Through-Skull Fluorescence Imaging of the Brain in a New Near-Infrared Window. *Nat. Photonics* **2014**, 8, 723-730.
- Bruns, O. T.; Bischof, T. S.; Harris, D. K.; Franke, D.; Shi, Y.; Riedemann, L.; Bartelt, A.; Jaworski, F. B.; Carr, J. A.; Rowlands, C. J., Next-Generation *In Vivo* Optical Imaging with Short-Wave Infrared Quantum Dots. *Nat. Biomed. Eng.* **2017**, 1, 0056.
- Ren, F.; del Rosal, B.; An, S. Y.; Yang, F.; Carrasco, E.; Benayas, A.; Oh, J. K.; Jaque, D.; de la Fuente, Á. J.; Vetrone, F., Development and Investigation of Ultrastable PbS/CdS/ZnS Quantum Dots for Near - Infrared Tumor Imaging. *Particle & Particle Systems Characterization* **2017**, 34, 1600242

15. Tao, Z.; Dang, X.; Huang, X.; Muzumdar, M. D.; Xu, E. S.; Bardhan, N. M.; Song, H.; Qi, R.; Yu, Y.; Li, T.; Wei, W.; Wyckoff, J.; Birrer, M. J.; Belcher, A. M.; Ghoroghchian, P. P., Early Tumor Detection Afforded by *In Vivo* Imaging of Near-Infrared II Fluorescence. *Biomaterials* **2017**, *134*, 202-215.
16. Chan, W. C. W.; Maxwell, D. J.; Gao, X.; Bailey, R. E.; Han, M.; Nie, S., Luminescent Quantum Dots for Multiplexed Biological Detection and Imaging. *Curr. Opin. Biotechnol.* **2002**, *13*, 40-46.
17. Mansfield, J. R.; Gossage, K. W.; Hoyt, C. C.; Levenson, R. M., Autofluorescence Removal, Multiplexing, and Automated Analysis Methods for *In-Vivo* Fluorescence Imaging. *J. Biomed. Opt.* **2005**, *10*, 041207.
18. Matschulat, A.; Drescher, D.; Kneipp, J., Surface-Enhanced Raman Scattering Hybrid Nanoprobe Multiplexing and Imaging in Biological Systems. *ACS Nano* **2010**, *4*, 3259-3269.
19. Li, Y.; Cu, Y. T. H.; Luo, D., Multiplexed Detection of Pathogen DNA with DNA-Based Fluorescence Nanobarcodes. *Nat. Biotechnol.* **2005**, *23*, 885-889.
20. Heinzmann, K.; Carter, L. M.; Lewis, J. S.; Aboagye, E. O., Multiplexed Imaging for Diagnosis and Therapy. *Nat. Biomed. Eng.* **2017**, *1*, 697.
21. Abbasi, A. Z.; Amin, F.; Niebling, T.; Friede, S.; Ochs, M.; Carregal-Romero, S.; Montenegro, J.-M.; Rivera Gil, P.; Heimbrodt, W.; Parak, W. J., How Colloidal Nanoparticles Could Facilitate Multiplexed Measurements of Different Analytes with Analyte-Sensitive Organic Fluorophores. *ACS Nano* **2011**, *5*, 21-25.
22. Hall, D. J.; Han, S. In *Preliminary Results from a Multi-Wavelength Time Domain Optical Molecular Imaging System*, Proc. SPIE, 2007; p 64300T.
23. Hall, D. J.; Sunar, U.; Farshchi-Heydari, S.; Han, S.-H., In Vivo Simultaneous Monitoring of Two Fluorophores with Lifetime Contrast Using a Full-Field Time Domain System. *Appl. Opt.* **2009**, *48*, D74-D78.
24. Lu, Y.; Zhao, J.; Zhang, R.; Liu, Y.; Liu, D.; Goldys, E. M.; Yang, X.; Xi, P.; Sunna, A.; Lu, J., Tunable Lifetime Multiplexing Using Luminescent Nanocrystals. *Nat. Photonics* **2014**, *8*, 32-36.
25. Berezin, M. Y.; Achilefu, S., Fluorescence Lifetime Measurements and Biological Imaging. *Chem. Rev.* **2010**, *110*, 2641-2684.
26. Dong, H.; Sun, L.-D.; Feng, W.; Gu, Y.; Li, F.; Yan, C.-H., Versatile Spectral and Lifetime Multiplexing Nanoplatform with Excitation Orthogonalized Upconversion Luminescence. *ACS Nano* **2017**, *11*, 3289-3297.
27. Jin, D.; Piper, J., Time-Gated Luminescence Microscopy Allowing Direct Visual Inspection of Lanthanide-Stained Microorganisms in Background-Free Condition. *Anal. Chem.* **2011**, *83*, 2294-2300.
28. Lu, Y.; Lu, J.; Zhao, J.; Cusido, J.; Raymo, F. M.; Yuan, J.; Yang, S.; Leif, R. C.; Huo, Y.; Piper, J. A.; Paul Robinson, J.; Goldys, E. M.; Jin, D., On-The-Fly Decoding Luminescence Lifetimes in the Microsecond Region for Lanthanide-Encoded Suspension Arrays. *Nat. Commun.* **2014**, *5*, 3741.
29. Hoffmann, K.; Behnke, T.; Drescher, D.; Kneipp, J.; Resch-Genger, U., Near-Infrared-Emitting Nanoparticles for Lifetime-Based Multiplexed Analysis and Imaging of Living Cells. *ACS Nano* **2013**, *7*, 6674-6684.
30. del Rosal, B.; Ortgies, D. H.; Fernández, N.; Sanz - Rodríguez, F.; Jaque, D.; Rodríguez, E. M., Overcoming Autofluorescence: Long - Lifetime Infrared Nanoparticles for Time - Gated *In Vivo* Imaging. *Adv. Mater.* **2016**, *28*, 10188-10193.
31. Zheng, X.; Zhu, X.; Lu, Y.; Zhao, J.; Feng, W.; Jia, G.; Wang, F.; Li, F.; Jin, D., High-Contrast Visualization of Upconversion Luminescence in Mice Using Time-Gating Approach. *Anal. Chem.* **2016**, *88*, 3449-3454.
32. Jin, D.; Lu, Y.; Leif, R. C.; Yang, S.; Rajendran, M.; Miller, L. W. How to Build a Time-Gated Luminescence Microscope. In *Current Protocols in Cytometry*; John Wiley & Sons, Inc.: Hoboken, NJ, USA, 2014; pp. 2.22.1-2.22.36.
33. Yang, M.; Liang, Y.; Gui, Q.; Zhao, B.; Jin, D.; Lin, M.; Yan, L.; You, H.; Dai, L.; Liu, Y., Multifunctional Luminescent Nanomaterials from NaLa(MoO₄)(2):Eu(3+)/Tb(3+) with Tunable Decay Lifetimes, Emission Colors, and Enhanced Cell Viability. *Sci. Rep.* **2015**, *5*, 11844.
34. Balogh, L.; Nigavekar, S. S.; Nair, B. M.; Lesniak, W.; Zhang, C.; Sung, L. Y.; Kariapper, M. S.; El-Jawahri, A.; Llanes, M.; Bolton, B.; Mamou, F.; Tan, W.; Hutson, A.; Minc, L.; Khan, M. K., Significant Effect of Size on the *In Vivo* Biodistribution of Gold Composite Nanodevices in Mouse Tumor Models. *Nanomedicine* **2007**, *3*, 281-296.
35. Alexis, F.; Pridgen, E.; Molnar, L. K.; Farokhzad, O. C., Factors Affecting the Clearance and Biodistribution of Polymeric Nanoparticles. *Mol. Pharm.* **2008**, *5*, 505-515.
36. Chen, G. Y.; Shen, J.; Ohulchanskyy, T. Y.; Patel, N. J.; Kutikov, A.; Li, Z. P.; Song, J.; Pandey, R. K.; Agren, H.; Prasad, P. N.; Han, G., (alpha-NaYbF₄:Tm³⁺)/CaF₂ Core/Shell Nanoparticles with Efficient Near-Infrared to Near-Infrared Upconversion for High-Contrast Deep Tissue Bioimaging. *ACS Nano* **2012**, *6*, 8280-8287.
37. Villa, I.; Vedda, A.; Cantarelli, I. X.; Pedroni, M.; Piccinelli, F.; Bettinelli, M.; Speghini, A.; Quintanilla, M.; Vetrone, F.; Rocha, U.; Jacinto, C.; Carrasco, E.; Sanz-Rodríguez, F.; Juarranz, Á.; del Rosal, B.; Ortgies, D. H.; Haro Gonzalez, P.; García Solé, J.; Jaque García, D., 1.3 μm Emitting SrF₂:Nd³⁺ Nanoparticles for High Contrast *In Vivo* Imaging in the Second Biological Window. *Nano Res.* **2015**, *8*, 649-665.



In vivo infrared multiplexed images are obtained by using rare-earth-doped nanoparticles with tunable fluorescence lifetime. A combination of time-gating, time-domain image analysis and engineering of the rare-earth-doping contributes towards multiplexed imaging and diagnostic procedures in the second biological window.